Princeton Plasma Physics Laboratory

PPPL- 4937

PPPL- 4937

Gyrokinetic Particle Simulation of Nonlinear Evolution of Mirror Instability

Peter Porazik and Jay R. Johnson

AUGUST, 2013

PPPL PRINCETON PLASMA PHYSICS LABORATORY

Prepared for the U.S. Department of Energy under Contract DE-AC02-09CH11466.

Princeton Plasma Physics Laboratory
Report Disclaimers

Full Legal Disclaimer

Trademark Disclaimer

PPPL Report Availability

Princeton Plasma Physics Laboratory:

http://www.pppl.gov/techreports.cfm

Office of Scientific and Technical Information (OSTI):

http://www.osti.gov/bridge

Related Links:

U.S. Department of Energy

Office of Scientific and Technical Information

Fusion Links

Gyrokinetic particle simulation of nonlinear evolution of mirror instability.

Peter Porazik,[1] Jay R. Johnson[1]

Abstract. A gyrokinetic simulation model for nonlinear studies of the mirror instability is described. The model is set in a uniform, periodic slab with anisotropic ions and cold electrons. Particle-in-cell simulations with a noise reducing δf algorithm show agreement with the linear theory of the mirror instability. Results of nonlinear simulations near marginal stability are presented. Single-mode simulations show saturation due to trapping. Simulations with a spectrum of unstable modes show that the negative magnetic perturbations saturate at a lower amplitude and earlier than the positive magnetic perturbations, which results in the development of peaked saturated structures. The saturation amplitude of negative magnetic perturbations is in agreement with the trapped particle theory, while the saturation amplitude of the positive magnetic perturbations is determined by the local change in the $\beta_\perp$ (ratio of perpendicular plasma pressure to magnetic pressure) parameter.

1. Introduction

Mirror instability is a phenomenon observed in magnetized plasmas with high plasma pressure, and the temperature along the magnetic field line less than the temperature perpendicular to it. Its initiation can be understood as due to the diamagnetic plasma moving into regions of weak magnetic field, and there further reducing its amplitude [*Hasegawa*, 1969]. One of the characterstic properties of the mirror mode is the out of phase relationship between the magnetic and plasma pressures. In a spatially uniform plasma the mode has zero frequency, even in the stable regime [*Tajiri*, 1967; *Hasegawa*, 1969]. In addition, the linear growth rate is inversely proportional to the number of resonant particles, those whose velocity parallel to the magnetic field is equal to zero [*Southwood and Kivelson*, 1993]. For these reasons, the mirror instability is considered to be a kinetic instability, and is not associated with shear Alfven, compressional, or the acoustic waves of the fluid theory [*Hasegawa*, 1969; *Southwood and Kivelson*, 1993]. The nonlinear evolution of the mirror instability remains a subject of current research, which aims to answer how the amplitude of the mirror instability saturates and what governs the development of the saturated magnetic structures [*Pantellini et al.*, 1995; *Kivelson and Southwood*, 1996; *Pantellini*, 1998; *Califano et al.*, 2008; *Hellinger et al.*, 2009; *Jovanović and Shukla*, 2009; *Pokhotelov et al.*, 2010]. The interest in these questions is motivated by satellite observations, which consistently find stationary magnetic structures with mirror mode properties in planetary magnetospheres, and the solar wind [*Winterhalter et al.*, 1995; *Johnson and Cheng*, 1997; *Joy et al.*, 2006; *Soucek et al.*, 2008; *Korotova et al.*, 2009; *Génot et al.*, 2009a; *Balikhin et al.*, 2010; *Enríquez-Rivera et al.*, 2010; *Tsurutani et al.*, 2011].

The purpose of this paper is to describe a gyrokinetic simulation model for the mirror instability in order to help answer these questions. The gyrokinetic theory applies to wave phenomena whose frequencies are lower than the gyrofrequency, but whose wave lengths may be the order of the Larmor radius. Within this domain, gyrokinetic simulation codes are more efficient than their fully kinetic counterparts, because they do not resolve the fast gyromotion of the particles around the magnetic field. The advantage is further amplified near an instability threshold, where the wave evolution may be especially slow. We therefore apply the gyrokinetic simulation to study the development of the mirror instability. The model we describe is reduced, in the sense that it does not contain all the physics present in the full gyrokinetic theory, but attempts to isolate the dominant components thought to be responsible for mirror mode dynamics. The reductions also dramatically simplify the simulation. Thus, within the model the electrons are treated as a massless cold fluid, shorting out the parallel electric field; collisions are ignored; and only the co-planar (in the plane of the wave-vector and the background magnetic field) magnetic perturbations are considered.

A gyrokinetic simulation model for the mirror instability has been described previously by *Qu et al.* [2007, 2008]. In *Qu et al.* [2007], the gyrokinetic version of the linear dispersion relation was derived, and successfully used for verification of the gyrokinetic particle-in-cell (PIC) simulation code. *Qu et al.* [2008] reports on nonlinear simulations which demonstrated saturation of a single unstable mode due to particle trapping. We verify our simulations against these results and provide extension to the regime with a spectrum of unstable modes. Other differences from the model described in these papers have to do with ordering and numerical implementation, and will be addressed in following sections.

The model is described in Section 2, which contains the theoretical framework and comparisons with existing models. The simulation methods and results are described in Section 3. The last section summarizes the simulation results, and attempts to explain their features.

2. Model Formulation

The model consists of the collisionless ion gyrokinetic equation and the perpendicular Ampere's law. Electrons are cold, providing no contribution to the perpendicular current and shorting out the electric field parallel to the background magnetic field, $E_\parallel = 0$. The magnetic perturbations are coplanar, in the **B**-**k** plane, where **B** is the background magnetic field and **k** is the wave vector. The coplanarity assumption is commonly used in investigations of the mirror instability, and its validity regime has been studied by

[1]Princeton Plasma Physics Laboratory, Princeton University, Princeton, New Jersey, USA.

0148-0227/13/$9.00

Génot et al. [2001], who found it to be most correct when the anisotropy and plasma beta are low. The perpendicular Ampere's law establishes the relationship between magnetic perturbation and perpendicular ion pressure; and $\nabla\cdot\delta\mathbf{B}=0$ relates the parallel and perpendicular components of the perturbed magnetic field. The geometry of the model is that of a uniform slab with periodic boundary conditions.

Designating the wave frequency by ω, the ion cyclotron frequency by $\Omega_i = eB/mc$, wave-vector perpendicular to the magnetic field by $k_\perp$, and the ion Larmor radius by $\rho_i = \sqrt{T_\perp/m}/\Omega_i$, the classical gyrokinetic theory is based on the ordering $\omega/\Omega_i \sim O(\epsilon) \ll 1$, and $k_\perp\rho_i \sim O(1)$. The gyrokinetic ion response to coplanar magnetic perturbations is then governed by

$$\partial_t F + \dot{\mathbf{X}}\cdot\partial_{\mathbf{X}}F + \dot{v}_\parallel\partial_{v_\parallel}F = 0, \tag{1}$$

where, to $O(\epsilon)$, the equations of motion are [*Brizard*, 1992, 1989],

$$\dot{\mathbf{X}} = v_\parallel\left(\hat{\mathbf{b}} + \frac{\langle\delta\mathbf{B}_\perp(\mathbf{x})\rangle}{B}\right) + \frac{c}{eB}\hat{\mathbf{b}}\times\nabla\mu\left\langle\left\langle\delta B_\parallel(\mathbf{x})\right\rangle\right\rangle \tag{2}$$

$$\dot{v}_\parallel = -\frac{\mu}{m}\left(\hat{\mathbf{b}} + \frac{\langle\delta\mathbf{B}_\perp(\mathbf{x})\rangle}{B}\right)\cdot\nabla\left\langle\left\langle\delta B_\parallel(\mathbf{x})\right\rangle\right\rangle. \tag{3}$$

$F(\mathbf{X}, v_\parallel, \mu)$ is the gyrocenter distribution function, whose formal dependance on the gyroangle ξ has been removed due to the frequency ordering, and $\mathbf{X}$ is the gyrocenter position, $v_\parallel$ is the parallel gyrocenter velocity, and μ is the gyrocenter magnetic moment. The magnetic moment is a conserved quantity, $\dot{\mu}=0$. The background magnetic field, B, is uniform and points in the $\hat{\mathbf{b}}$ direction. The magnetic perturbation parallel to the background magnetic field is designated by $\delta B_\parallel$, and perpendicular to it by $\delta\mathbf{B}_\perp$. The gyro-angle averaging operation is $\langle\ ...\ \rangle \equiv \frac{1}{2\pi}\int_0^{2\pi}\ ...\ d\xi$, and $\langle\langle\ ...\ \rangle\rangle$ stands for the operation $\frac{1}{\pi\rho^2}\int_0^{2\pi}\int_0^{\rho}\ ...\ rdrd\xi$, i.e. averaging over the surface enclosed by the gyro-orbit of radius $\rho = v_\perp/\Omega_i = \sqrt{2\mu B/m}/\Omega_i$. The first term of equation (2) corresponds to the velocity along the total magnetic field (unperturbed + perturbed), and the second term corresponds to the perturbed magnetic gradient drift. Equation (3) describes the mirror force along the total magnetic field, due to the parallel magnetic perturbation.

The field equation used to close the system is derived from the perpendicular Ampere's law,

$$\frac{\delta B_\parallel B}{4\pi}\left(1+\frac{k_\parallel^2}{k_\perp^2}\right) = -2\pi\int\frac{B}{m}dv_\parallel d\mu\frac{2}{k_\perp\rho}J_1(k_\perp\rho)\mu B\left(\delta F - \mu\frac{\left\langle\left\langle\delta B_\parallel\right\rangle\right\rangle}{B}\frac{\partial F_0}{\partial\mu}\right), \tag{4}$$

where J_1 is the 1st order Bessel Function, F_0 is the background particle distribution function, and $k_\parallel$ is the wave number parallel to the magnetic field.

Equation (4) resembles the low-frequency force balance equation whose details of derivation may be found in *Brizard* [1989, 1992]; *Brizard and Hahm* [2007]; *Porazik and Lin* [2011]. The only difference from previous gyrokinetic derivations is the inclusion of the $k_\parallel^2/k_\perp^2$ term whose origin is the contribution of the coplanar perpendicular magnetic perturbations, $\delta\mathbf{B}_\perp$, which was expressed in terms of $\delta B_\parallel$ using $\nabla\cdot\delta\mathbf{B}=0$. As it is common to use the ordering $k_\parallel/k_\perp \ll 1$ in gyrokinetic formulations, this term is usually ordered out of the field equations. However, the more general requirement is that $k_\parallel v_\parallel/\Omega_i \ll 1$, which turns into the former relation for models with temperature isotropy and most unstable modes at $k_\perp\rho_i\sim 1$. For the mirror instability, sufficiently close to threshold $k_\parallel v_\parallel/\Omega_i \ll 1$ is satisfied while $k_\parallel/k_\perp \ll 1$ may not be.

The physics introduced by this term in this model corresponds to stabilization of mirror modes due to field line tension. The right-hand side of equation (4) corresponds to the ion kinetic pressure, and is composed of two terms. The first term is the perturbed gyrokinetic ion pressure, where $\delta F \equiv F - F_0$ is the perturbed gyrocenter distribution function. The second term corresponds to the magnetization effects introduced by the transformation between gyrocenter coordinates and particle coordinates.

Linearizing the gyrokinetic equation (1), and using a bi-Maxwellian distribution for F_0

$$F_0 = n_0\sqrt{\frac{m^3}{(2\pi)^3T_\perp^2T_\parallel}}e^{-(mv_\parallel^2/2T_\parallel + \mu B/T_\perp)}. \tag{5}$$

the linear dispersion relation for the mirror instability is obtained,

$$1+\left(\frac{k_\parallel}{k_\perp}\right)^2 - \frac{T_\perp}{T_\parallel}\left[\beta_\perp - \beta_\parallel + \beta_\perp\frac{\omega}{\sqrt{2}k_\parallel v_{th\parallel}}Z\left(\frac{\omega}{\sqrt{2}k_\parallel v_{th\parallel}}\right)\right] \times\left[I_0(k_\perp^2\rho_i^2) - I_1(k_\perp^2\rho_i^2)\right]e^{-k_\perp^2\rho_i^2} = 0, \tag{6}$$

where $\beta_{\perp,\parallel} = 8\pi n_0 T_{\perp,\parallel}/B^2$, Z is the plasma dispersion function, $v_{th\parallel} = \sqrt{T_\parallel/m}$ and I_n is the Modified Bessel Function of the 1st kind. The dispersion relation is in agreement with equation (35) of *Hasegawa* [1969] for the case of uniform background. The finite Larmor radius effects do not change the instability threshold condition, which is $\beta_\perp A > 1$ where $A \equiv T_\perp/T_\parallel - 1$, but they do determine the value of the maximum growth rate.

The mirror instability was previously studied using gyrokinetic particle simulations by *Qu et al.* [2007, 2008]. The model was slightly different, in that it contained an additional stabilizing term due to the combined effect of field-line tension, anisotropy, and finite Larmor radius effects. The term however has no affect on the instability threshold, and only a slight effect on the growth rate. Within the framework of gyrokinetics, the term may be derived by solving for the phase space gauge function, S, to higher order in $k_\parallel v_\parallel/\Omega_i$. [*Qin*, 1998] Further discussion of this term and the higher order gauge function, S, is given in the Appendix.

Energy conservation for this model may be demonstrated by taking the second moment of the gyrokinetic equation with respect to $v_\parallel$, integrating over the entire phase-space, and then substituting the perpendicular Ampere's law to obtain

$$\frac{1}{8\pi}\int\left(\delta B_\parallel^2 + \delta B_\perp^2\right)d\mathbf{x} + \int\left(\frac{mv_\parallel^2}{2} + \mu\delta B_\parallel\right)Fd^6\mathbf{Z} + \frac{\beta_i}{8\pi}\sum_k\left[I_0\left(k_\perp^2\rho_i^2\right) + I_1\left(k_\perp^2\rho_i^2\right)\right]e^{-k_\perp^2\rho_i^2}\delta B_{\parallel k}^2 = 0. \tag{7}$$

Equation (7) is a sum of three terms. The first term corresponds to the change in magnetic field energy. The next two terms correspond to the change in gyrokinetic energy of ions and the correction due to magnetization effects, respectively. The sum of these terms corresponds to the change in total energy and is equal to zero. More details about the energy conservation in gyrokinetic formulations which include the compressional magnetic component $\delta B_\parallel$ may be found in *Hahm et al.* [2009] and *Brizard* [2010].

3. Simulation Description

The mirror mode model was simulated using the particle-in-cell (PIC) technique. The δf-scheme[1] was used to reduce the particle noise [*Parker and Lee*, 1993; *Aydemir*, 1994; *Hu and Krommes*, 1994]. The simulation particles (marker-particles) therefore represent only the perturbed part of the total gyrocenter distribution function. Linear interpolation was used between the marker particles and the grid. The ion gyrocenters move in the three dimensional periodic box according to their equations of motion given by (2-3). The gyro-averaging operations are performed for each gyrocenter by averaging over points along the gyro-orbit, as described in *Lee* [1983]; *Porazik and Lin* [2011]. In simulations presented in this paper, 4 points were used to perform the gyro-averaging operations, an approximation suitable for $k_\perp \rho_i < 2$. This method is facilitated by expressing the model in terms of $\delta B_\parallel$, which enables gyro-averaging directly on this scalar quantity. An alternative is to use $\delta \mathbf{A}_\perp$, and perform the gyro-average on $\langle \delta \mathbf{A} \cdot \mathbf{v}_\perp \rangle$. This method was described in *Lee and Qin* [2003] and implemented by *Qu et al.* [2008].

The pressure contributions of each gyrocenter are deposited on the grid by linear interpolation. The pull-back transformation into particle coordinates, which is the origin of the $2J_1(k_\perp \rho)/k_\perp \rho$ factor in (4), is also performed using the 4-point averaging in real space. The magnetization term in equation (4) is estimated by analytically performing the integral with the assumption of a bi-Maxwellian distribution. The equation is then solved for $\delta B_\parallel$ in the Fourier space, keeping only those Fourier spectral components whose perpendicular wave vector is in the same direction as the perpendicular magnetic perturbation, thus reducing the solution to two dimensions. The spatial average of the magnetic perturbation is therefore always zero. The initial marker-particle distribution in each simulation was bi-Maxwellian, and the simulations were initialized with low amplitude random noise. The simulation code was parallelized using MPI and OpenMP.

Figure 1 shows results of a simulation in which only a single, most unstable, spectral component was kept, while all others were filtered out. The simulation was initialized with unstable parameters, $\beta_\parallel = 0.251$ and $T_\perp/T_\parallel = 6$, giving $\beta_\perp A = 7.5$. The expected linear growth rate for these parameters is $\gamma = 0.133\Omega_i$, and the simulation showed the growth rate to be $\approx 0.132\Omega_i$. The parameters later evolve into a less stable regime of $\beta_\perp A \approx 5.5$, but never relax to marginal stability, and instead oscillations appear in the saturated regime. These oscillations are due to trapped particles bouncing between the wave crests, repeatedly taking and giving energy to the wave at approximately the rate of its linear growth. The frequency of these oscillations is $\approx 0.172\Omega_i$. Using the parallel wavelength of the unstable mode, $k_\parallel \rho_i \approx 0.544$, the saturation amplitude from the trapping theory [*O'Neil et al.*, 1971; *Nicholson*, 1983; *Pantellini et al.*, 1995; *Qu et al.*, 2007] is $\delta B/B = 2(\gamma/\Omega_i)^2/(k_\parallel \rho_i)^2 = 0.118$, which is close to the simulation result of $\delta B/B \approx 0.11$. These results are in agreement with gyrokinetic simulations of a single unstable mode reported by *Qu et al.* [2008], where saturation due to trapping was observed for $\beta_\perp A = 2$.

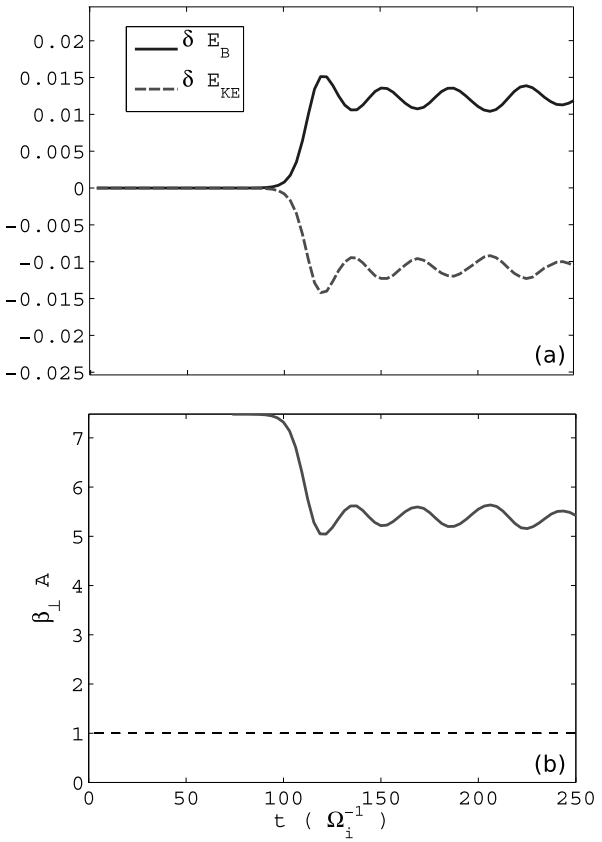

Figure 1. Figure (a) shows the change in magnetic (δE_B) and kinetic (δE_{KE}) energy, as a function of time. Figure (b) shows the change in the threshold parameter $\beta_\perp A$. These results were produced by a simulation in which only a single unstable mode was kept. The simulation was initialized with $\beta_\perp A = 7.5$.

Figures 2-8 summarize results of a simulation in which a spectrum of unstable modes was allowed. The size of the simulation box was $1256.6\rho_i$ in the z-direction (along background field), and $228.4\rho_i$ in the x- and y-directions. The number of grid points in the z direction was 512, and in the x direction it was 256. The number of marker particles was 64×10^6. The initial parameters in this simulation were $\beta_\parallel = 0.0718$ and $T_\perp/T_\parallel = 6$, giving $\beta_\perp A = 2.154$. Figure 2 (a) shows the evolution of magnetic and kinetic energies. Figure 2 (b) shows that the global stability parameter $\beta_\perp A$ for a bi-Maxwellian plasma only changes by a few percent throughout the simulation, and thus according to this parameter the plasma remains unstable. The evolution may be separated into two stages. In the first stage, the most unstable mode of the spectrum grows until it is halted at $t \approx 900\Omega_i^{-1}$. The tendency towards nonlinear oscillations may be identified at this time in Figure 2 (a), and the amplitude of the magnetic perturbation at this point scales in accordance with the trapped particle theory. The growth rate in the linear stage was $\gamma \approx 0.0129\Omega_i$, and the wave vector in the parallel direction was $k_\parallel \rho_i \approx 0.1234$. The saturation level from the trapping theory should therefore be $2(\gamma/\Omega_i)^2/(k_\parallel \rho_i)^2 = \delta B/B \approx 0.0219$. The magnetic field amplitude at $t \sim 900\Omega_i^{-1}$ of the simulation, which corresponds to the initial trapping stage, is $\delta B/B \approx 0.0226$.

As can be seen from Figure 2 (a), the amplitude of the magnetic field continues to grow after $t \approx 900\Omega_i^{-1}$ until the

end of the simulation, however at a progressively lower rate. The magnetic structure along the z-direction at $t = 900\Omega_i^{-1}$ and at the end of the simulation, at $t = 2775\Omega_i^{-1}$, is shown in Figure 3. The negative perturbations (troughs) of the structure remain roughly at the same level between the two times, while the amplitude of the positive perturbations (crests) is increased. Figure 4 shows the average skewness[*Soucek et al.*, 2008; *Génot et al.*, 2009b] of the magnetic structure along the z-direction, demonstrating the development of peaked structures after $t \approx 900\Omega_i^{-1}$. In addition to increasing in amplitude, the magnetic structure also increases in length scale. The dominant increase in length scale is however by the negative perturbations, balancing out the positive perturbations so that the average perturbation is zero. This effect is demonstrated in Figure 5 which shows the time evolution of the magnetic structure along the z-direction at a particular value of x, designated with the dashed line in the top panel. Before $t \approx 900\Omega_i^{-1}$ the scale of the crests and trough is approximately the same. After this time, the increase in the scale of the troughs is larger than that of the crests. The final structure thus contains wide shallow troughs, followed by peaked narrow crests.

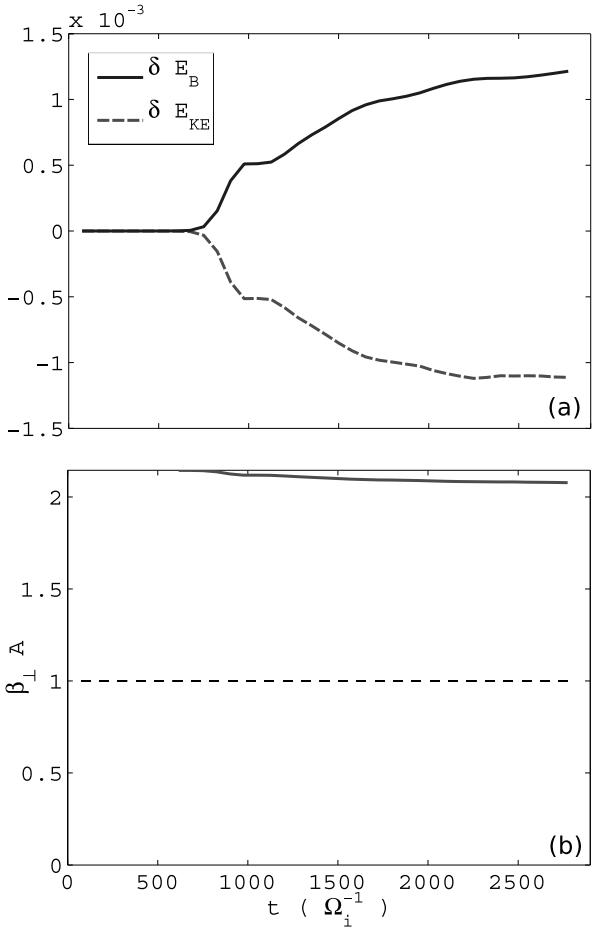

Figure 2. Figure (a) shows the change of magnetic (δE_B) and kinetic (δE_{KE}) energies, as a function of time. Figure (b) shows the change in the threshold parameter $\beta_\perp A$. These results were produced by a simulation with a spectrum of unstable perturbations. The simulation was initialized with $\beta_\perp A = 2.154$.

The qualitative features of the perturbed gyrocenter distribution function δF at the end of a simulation, integrated in the z-direction, are shown in Figure 6. It can be seen that the distribution function is decreased near the resonant location $v_\parallel \approx 0$, and is increased near the trapping boundary, showed by the dashed line. The perturbed gyrocenter distribution at the location of the crests and troughs is plotted in Figure 7, as a function of $v_\parallel$. While the distribution function is decreased at the location of crests ($\delta B > 0$), it is flattened at the location of troughs ($\delta B < 0$). This suggests that, while the saturation of the troughs is due to trapping, the crests saturate due to local decrease in $\beta_\perp$ as a result of the decrease in density and increase in magnetic field. Assuming that the instability threshold parameter $\beta_\perp A$ only changes due to $\beta_\perp$, the change in $\beta_\perp$ required to reach the marginal stability may be estimated as $\delta\beta_\perp/\beta_\perp \approx \delta n/n - 2\delta B/B = (1 - \beta_\perp A)/\beta_\perp A \approx -0.536$, with $\beta_\perp A = 2.154$. The bottom panel of Figure 8 shows $\delta\beta_\perp$ as a function of z, along with the threshold level (dashed line). The change of $\beta_\perp$ at the location of magnetic peaks is thus seen to approach the threshold.

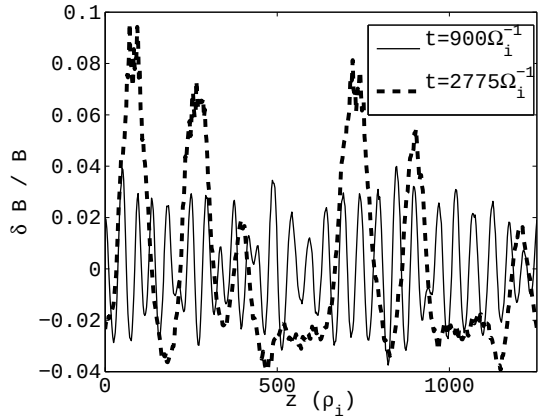

Figure 3. The figure shows the mode structure along the z-direction at two different times corresponding to the early nonlinear stage (thin, solid line), and the final stage of the simulation (thick, dashed line).

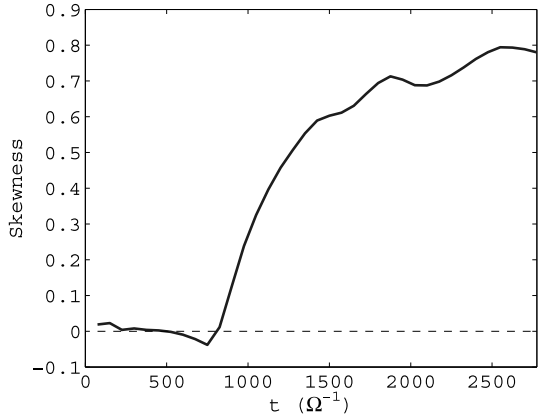

Figure 4. The figure shows the evolution of the average skewness of the magnetic structure. The average was taken in the x-direction, at each time step.

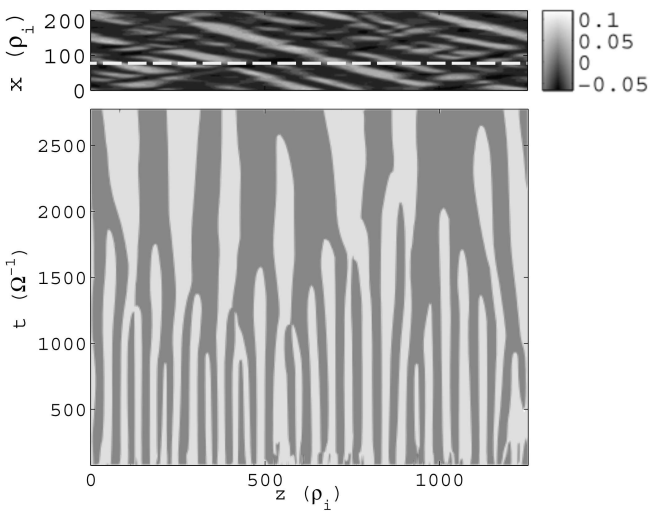

Figure 5. The top panel shows the magnetic structure (δB) in the x-z plane at the end of the simulation, and the dashed line marks the location at which the lower plot was constructured. The lower plot shows the evolution of the scale of the magnetic structure in the z-direction, at the particular value of x, as a function of time. The light colors correspond to positive perturbations and the darker colors to negative perturbations.

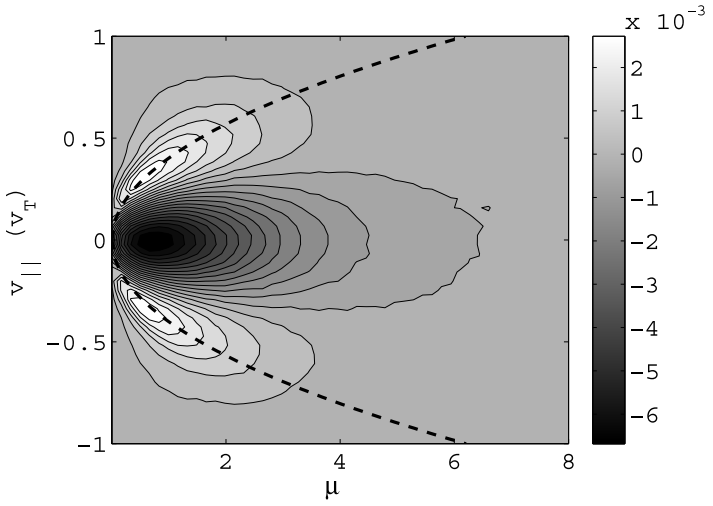

Figure 6. Shown is the perturbed gyrocenter distribution function (δF) in the μ-$v_\parallel$ plane, at the end of the simulation. The dashed curve corresponds to the approximate trapped-passing boundary of the particles.

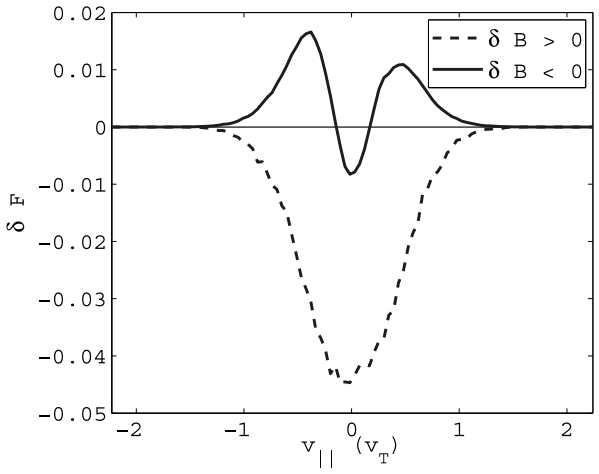

Figure 7. The figure shows the perturbed gyrocenter distribution function at the location of positive magnetic perturbations (dashed) and negative magnetic perturbations (solid), as a function of $v_\parallel$.

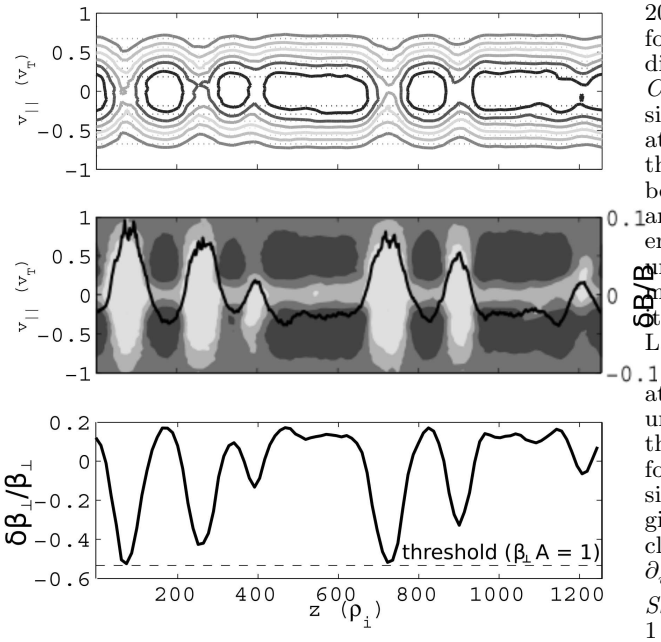

Figure 8. The top plot shows the contours of the total gyrocenter distribution function F in the z-$v_\parallel$ plane at the final stage of the simulation. The straight dotted lines designate the contours of the initial distribution, F_0. The center plot shows the perturbed distribution function δF. The darker/lighter colors designate positive/negative values. Superimposed in the black solid line is the magnetic perturbation δB, whose axis is on the right hand side. The bottom plot shows the perturbation in density, along with the instability threshold level (dashed line).

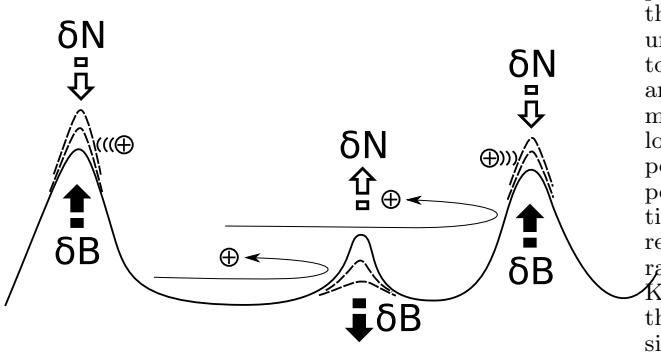

Figure 9. Summary of the development of the saturated mirror mode structure.

4. Discussion

A gyrokinetic simulation model for the mirror instability has been described. The model isolates the physics governing the evolution of the mirror mode. Linear and non-linear simulations, with only the most unstable mode present, agree well with theoretical expectations, and previous works.[*Qu et al.*, 2007, 2008] When more modes are included, nonlinear simulations show saturation due to particle trapping, followed by further evolution of the mode structure into magnetic peaks. Magnetic peaks have also been observed in previous simulations,[*Baumgärtel et al.*, 2003; *Borgogno et al.*, 2007; *Califano et al.*, 2008] and their formation was attributed to "higher order finite Larmor radius effects," [*Kuznetsov et al.*, 2007; *Borgogno et al.*, 2007; *Califano et al.*, 2008] specifically the difference between the size of Larmor radii of ions located in the high field regions at the crests of the perturbation, and the low field regions in the troughs of the perturbation. This effect is considered to be of higher order in the gyrokinetic model described here, and is not included. (In performing the gyro-averaging operation, for example, the Larmor radius is found from the unperturbed background field only.) Nonetheless the formation of peaked structures was observed suggesting that it is due to a more robust process than higher order finite Larmor radius effects.

The simulations show that the amplitude of the negative magnetic perturbations saturates first. The saturation amplitude agrees with the estimate based on the trapping theory, $\delta B/B = 2(\gamma/\Omega_i)^2/(k_\parallel \rho_i)^2$. Thus for the evolution of the dips it is important to consider the flattening of the distribution function at the region of phase space that corresponds to trapped particles. The flattening of the distribution function supresses $\partial_{v_\parallel^2} F$ in the generalized threshold condition,[*Shapiro and Shevchenko*, 1966; *Pokhotelov et al.*, 2005; *Hellinger*, 2007] $1 + \beta_\perp + 8\pi B/m^2 \mathrm{P} \int dv_\parallel d\mu \mu^2 \partial_{v_\parallel^2} F < 0$, leading to the saturation of the dips. Assessment of the stability of plasma by estimation of the parameter $\beta_\perp A$ alone would therefore be incomplete in this region of the magnetic structure. The amplitude of the positive magnetic perturbations continues to grow past the time of saturation of negative magnetic perturbations, which results in the formation of peaked structures. As the peaks ($\delta B > 0$) grow, the number of particles close to the resonance point, $v_\parallel \approx 0$, decreases at their location, while the number of particles at the location of magnetic dips ($\delta B < 0$) is increased. These features can be seen in Figure 6, which shows the perturbed gyrocenter distribution function in the $v_\parallel$-μ plane, along with the trapped-passing boundary; and Figure 7, which shows the perturbed gyrocenter distribution function at the location of the peaks and the dips separately. The peaks appear to saturate when $\beta_\perp$ within their location is sufficiently reduced to be close to the marginal stability level. Assuming that anisotropy remains approximately the same, this was estimated as $\delta\beta_\perp/\beta_\perp \approx \delta n/n - 2\delta B/B = (1 - \beta_\perp A)/\beta_\perp A$. The lower panel of Figure 8 shows that $\beta_\perp$ at the location of the peaks is indeed signifcantly reduced, and for the dominant peaks the reduction is close to the threshold level. The estimate of $\delta\beta_\perp$ may be used together with the force-balance relation, $\delta B/B = -(\beta_\perp/2)\delta n/n$, to approximate the saturation level of the peaks as $\delta B/B = (\beta_\perp A - 1)/(2A + \beta_\perp A)$. Knowing the saturation level of the dips, and the peaks, then determines the form of the saturated structure in the simulation, since the spatial average of the perturbation is zero.

We have noted that the estimates for the saturation levels given above also compare well against the results of hybrid PIC simulations near threshold, presented in Figure 2 of *Califano et al.* [2008]. The simulation parameters used to produce the figure were given as $\beta_\perp = 1.857$, and $T_\perp/T_\parallel = 1.857$. These parameters yield the maximum growth rate of $\gamma/\Omega_i \approx 0.005$, and $k_\parallel \rho_i \approx 0.09$. The above estimates thus predict the saturation level of the dips at $\delta B/B \sim 0.0064$, and the saturation level of the peaks at $\delta B/B \sim 0.12$, in agreement with the top left panel of the Figure 2.

The process of the saturated structure formation is summarized in Figure 9. Thus, the resonant particles are Fermi accelerated by the growing peaks. The number of particles between the dominant peaks is consequently increased. However, due to the increased diamagnetic pressure between the dominant peaks, the amplitude of the subdominant peaks is diminished down to the level of magnetic dips

which thereby increase in width. The diminishing subdominant peaks inside the newly forming, wide, dips, affect the plasma by betatron cooling.

Although the saturated mirror mode structures observed in the simulations are opposite in form to the deep magnetic holes predicted in *Kivelson and Southwood* [1996]; *Pantellini* [1998], many of the same concepts that were used to explain their formation appear to be applicable to the formation of the peaked magnetic structures as well. The important difference is that after the initial trapping stage, the depth of the magnetic dips does not significantly increase. Instead their width increases as the spectrum of the structure changes to lower and lower wave numbers. Furthermore, the manner in which the width of the wells increases is by suppression of subdominant peaks by the newly trapped particles.

Many improvements to the existing model, and numerical techniques, are possible. More physics may be included by relaxing the restriction of cold, isotropic electrons;[*Pantellini and Schwartz*, 1995; *Pokhotelov et al.*, 2000; *Istomin et al.*, 2009; *Kuznetsov et al.*, 2013] and uniform magnetic field. Furthermore, non-coplanar magnetic perturbations may also play an important role when anisotropy is large enough.[*Génot et al.*, 2001] From the numerical perspective, the perpendicular Ampere's law may be solved in the real-space instead of the Fourier space[*Porazik and Lin*, 2011], enabling a more consistent treatment of the magnetization term which was here estimated using a bi-Maxwellian distribution.

Appendix A

The model of *Qu et al.* [2007] includes an additional term that is not included in the finite Larmor radius model of *Hasegawa* [1969], or the model described in this paper. The term appears in the perpendicular Ampere's law, and results in the dispersion relation

$$\begin{aligned} &1+\left(\tfrac{k_\parallel}{k_\perp}\right)^2\left[1+\alpha_b\left(\beta_\perp-\beta_\parallel\right)\right] \\ &-\tfrac{T_\perp}{T_\parallel}\left[\beta_\perp-\beta_\parallel+\beta_\perp\tfrac{\omega}{\sqrt{2}k_\parallel v_{th\parallel}}Z\left(\tfrac{\omega}{\sqrt{2}k_\parallel v_{th\parallel}}\right)\right] \\ &\times\left[I_0(k_\perp^2\rho_i^2)-I_1(k_\perp^2\rho_i^2)\right]e^{-k_\perp^2\rho_i^2}=0, \end{aligned} \tag{A1}$$

where $\alpha_b\left(\beta_\perp-\beta_\parallel\right)$ is the additional term and $\alpha_b \equiv \int_0^\infty x^3 e^{-x^2/2z} J_1'^2(x)dx/z^2$, $z = k_\perp^2\rho_i^2$. In context of the gyrokinetic theory, the term may be obtained by keeping higher order corrections, in $k_\parallel v_\parallel/\Omega_i$, in the gauge function S. However, the term has no effect on the instability threshold for $\beta_\perp > \beta_\parallel$, and only has a small effect on the growth rate of the most unstable mode. The reason it does not affect the threshold is that it only changes the factor in front of the $k_\parallel/k_\perp$ term in the dispersion relation. The curve that encloses the unstable region in the $(k_\parallel, k_\perp)$ plane maybe be obtained by setting $\omega = 0$ in the dispersion relation, and is given by

$$k_\parallel = k_\perp\sqrt{\frac{\left(\beta_\perp A\left[I_0(k_\perp^2\rho_i^2)-I_1(k_\perp^2\rho_i^2)\right]e^{-k_\perp^2\rho_i^2}-1\right)}{\left[1+\alpha_b\left(\beta_\perp-\beta_\parallel\right)\right]}}. \tag{A2}$$

The area enclosed by the curve approaches zero as the unstable parameters approach the threshold. When the threshold is crossed, $k_\parallel$ becomes imaginary for all values of $k_\perp$, and no solution for an unstable mode exists. For the mirror instability, $\beta_\perp > \beta_\parallel$, and the denominator of the radical is always positive. Since the maximum of $\left[I_0(k_\perp^2\rho_i^2)-I_1(k_\perp^2\rho_i^2)\right]e^{-k_\perp^2\rho_i^2}$ is 1, the value of $k_\parallel$ may only be imaginary, for all values of $k_\perp$, if $\beta_\perp A < 1$. Thus the instability threshold remains the same and is not affected by the α_b term. (For $\beta_\perp < \beta_\parallel$, the firehose threshold condition is obtained, $1 < \left(\beta_\parallel - \beta_\perp\right)/2$, and is completely determined by the denominator of the radical.)

Acknowledgments. This manuscript has been authored by Princeton University under Contract Number DE-AC02-09CH11466 with the U.S. Department of Energy. The United States Government retains and the publisher, by accepting the article for publication, acknowledges that the United States Government retains a non-exclusive, paid-up, irrevocable, worldwide license to publish or reproduce the published form of this manuscript, or allow others to do so, for United States Government purposes.

Notes

1. Also known as Monte-Carlo with control-variates or variance reduction as noted by *Aydemir* [1994]

References

Aydemir, A. Y. (1994), A unified Monte-Carlo interpretation of particle simulations and applications to non-neutral plasmas, *Physics of Plasmas*, *1*(4), 822–831.

Balikhin, M. A., O. A. Pokhotelov, S. N. Walker, R. J. Boynton, and N. Beloff (2010), Mirror mode peaks: THEMIS observations versus theories, *Geophys. Res. Lett.*, *37*, 5104.

Baumgärtel, K., K. Sauer, and E. Dubinin (2003), Towards understanding magnetic holes: Hybrid simulations, *Geophys. Res. Lett.*, *30*, 1761.

Borgogno, D., T. Passot, and P. L. Sulem (2007), Magnetic holes in plasmas close to the mirror instability, *Nonlinear Processes in Geophysics*, *14*(4), 373–383.

Brizard, A. J. (1989), Nonlinear gyrokinetic Maxwell-Vlasov equations using magnetic coordinates, *J. Plasma Phys.*, *41*, 541–559.

Brizard, A. J. (1992), Nonlinear gyrofluid description of turbulent magnetized plasmas, *Phys. Fluids B*, *4*, 1213–1228.

Brizard, A. J. (2010), Exact energy conservation laws for full and truncated nonlinear gyrokinetic equations, *Physics of Plasmas*, *17*(4), 042,303.

Brizard, A. J., and T. S. Hahm (2007), Foundations of nonlinear gyrokinetic theory, *Rev. Mod. Phys.*, *79*(2), 421–468.

Califano, F., P. Hellinger, E. Kuznetsov, T. Passot, P. L. Sulem, and P. M. Trávníček (2008), Nonlinear mirror mode dynamics: Simulations and modeling, *Journal of Geophysical Research (Space Physics)*, *113*, 8219.

Enríquez-Rivera, O., X. Blanco-Cano, C. T. Russell, L. K. Jian, and J. G. Luhmann (2010), Mirror Mode Structures in the Solar Wind: STEREO Observations, *Twelfth International Solar Wind Conference*, *1216*, 276–279.

Génot, V., S. J. Schwartz, C. Mazelle, M. Balikhin, M. Dunlop, and T. M. Bauer (2001), Kinetic study of the mirror mode, *J. Geophys. Res.*, *106*, 21,611–21,622.

Génot, V., E. Budnik, C. Jacquey, I. Dandouras, and E. Lucek (2009a), Mirror Modes Observed with Cluster in the Earth's Magnetosheath: Statistical Study and IMF/Solar Wind Dependence, *Advances in Geosciences, Volume 14: Solar Terrestrial (ST)*, *14*, 263.

Génot, V., E. Budnik, P. Hellinger, T. Passot, G. Belmont, P. M. Trávníček, P.-L. Sulem, E. Lucek, and I. Dandouras (2009b), Mirror structures above and below the linear instability threshold: Cluster observations, fluid model and hybrid simulations, *Annales Geophysicae*, *27*, 601–615.

Hahm, T. S., L. Wang, and J. Madsen (2009), Fully electromagnetic nonlinear gyrokinetic equations for tokamak edge turbulence, *Physics of Plasmas*, *16*(2), 022,305.

Hasegawa, A. (1969), Drift mirror instability in the magnetosphere, *Physics of Fluids*, *12*(12), 2642–2650.

Hellinger, P. (2007), Comment on the linear mirror instability near the threshold, *Physics of Plasmas*, *14*(8), 082,105.

Hellinger, P., E. A. Kuznetsov, T. Passot, P. L. Sulem, and P. M. Trávníček (2009), Mirror instability: From quasi-linear diffusion to coherent structures, *Geophys. Res. Lett.*, *36*, 6103.

Hu, G., and J. A. Krommes (1994), Generalized weighting scheme for delta f particle-simulation method, *Physics of Plasmas*, *1*(4), 863–874.

Istomin, Y. N., O. A. Pokhotelov, and M. A. Balikhin (2009), Nonzero electron temperature effects in nonlinear mirror modes, *Physics of Plasmas*, *16*(12), 122,901.

Johnson, J. R., and C. Z. Cheng (1997), Global structure of mirror modes in the magnetosheath, *J. Geophys. Res.*, *102*, 7179–7190.

Jovanović, D., and P. K. Shukla (2009), Nonlinear gyrokinetic theory for steady-state mirror mode magnetic structures, *Physics of Plasmas*, *16*(8), 082,901.

Joy, S. P., M. G. Kivelson, R. J. Walker, K. K. Khurana, C. T. Russell, and W. R. Paterson (2006), Mirror mode structures in the Jovian magnetosheath, *Journal of Geophysical Research (Space Physics)*, *111*(A10), 12,212.

Kivelson, M. G., and D. J. Southwood (1996), Mirror instability II: The mechanism of nonlinear saturation, *J. Geophys. Res.*, *101*, 17,365–17,372.

Korotova, G. I., D. G. Sibeck, V. Kondratovich, V. Angelopoulos, and O. D. Constantinescu (2009), Themis observations of compressional pulsations in the dawn-side magnetosphere: a case study, *Annales Geophysicae*, *27*(10), 3725–3735.

Kuznetsov, E. A., T. Passot, and P. L. Sulem (2007), Dynamical Model for Nonlinear Mirror Modes near Threshold, *Physical Review Letters*, *98*(23), 235,003.

Kuznetsov, E. A., T. Passot, and P. L. Sulem (2013), Nonlinear mirror modes in the presence of hot electrons, *Soviet Journal of Experimental and Theoretical Physics Letters*, *96*, 642–649.

Lee, W. W. (1983), Gyrokinetic approach in particle simulation, *Physics of Fluids*, *26*(2), 556–562.

Lee, W. W., and H. Qin (2003), Alfven waves in gyrokinetic plasmas, *Physics of Plasmas*, *10*(8), 3196–3203.

Nicholson, D. R. (1983), *Introduction to Plasma Theory*, John Wiley & Sons Inc.

O'Neil, T. M., J. H. Winfrey, and J. H. Malmberg (1971), Nonlinear Interaction of a Small Cold Beam and a Plasma, *Physics of Fluids*, *14*, 1204–1212.

Pantellini, F. G. E. (1998), A model of the formation of stable nonpropagating magnetic structures in the solar wind based on the nonlinear mirror instability, *J. Geophys. Res.*, *103*, 4789.

Pantellini, F. G. E., and S. J. Schwartz (1995), Electron temperature effects in the linear proton mirror instability, *Journal of Geophysical Research*, *100*, 3539–3549.

Pantellini, F. G. E., D. Burgess, and S. J. Schwartz (1995), On the non-linear mirror instability, *Advances in Space Research*, *15*, 341–344.

Parker, S. E., and W. W. Lee (1993), A fully nonlinear characteristic method for gyrokinetic simulation, *Phys. Fluids B*, *5*(1), 77–86.

Pokhotelov, O. A., M. A. Balikhin, H. S.-C. K. Alleyne, and O. G. Onishchenko (2000), Mirror instability with finite electron temperature effects, *Journal of Geophysical Research*, *105*, 2393–2402.

Pokhotelov, O. A., M. A. Balikhin, R. Z. Sagdeev, and R. A. Treumann (2005), Halo and mirror instabilities in the presence of finite Larmor radius effects, *Journal of Geophysical Research (Space Physics)*, *110*(A9), 10,206.

Pokhotelov, O. A., R. Z. Sagdeev, M. A. Balikhin, V. N. Fedun, and G. I. Dudnikova (2010), Nonlinear Mirror and Weibel modes: peculiarities of quasi-linear dynamics, *Annales Geophysicae*, *28*, 2161–2167.

Porazik, P., and Z. Lin (2011), Gyrokinetic simulation of magnetic compressional modes in general geometry, *Commun. Comput. Phys.*, *10*, 899.

Qin, H. (1998), Gyrokinetic theory and computational methods for electromagnetic perturbations in tokamaks, Phd. thesis, Princeton University.

Qu, H., Z. Lin, and L. Chen (2007), Gyrokinetic theory and simulation of mirror instability, *Physics of Plasmas*, *14*(4), 042,108.

Qu, H., Z. Lin, and L. Chen (2008), Nonlinear saturation of mirror instability, *Geophys. Res. Lett.*, *35*(10), L10,108.

Shapiro, V. D., and V. I. Shevchenko (1966), Quasilinear theory of instability of a plasma with anisotropic ion velocity distribution, *Plasma Physics and Controlled Thermonuclear Fusion*, p. 149.

Soucek, J., E. Lucek, and I. Dandouras (2008), Properties of magnetosheath mirror modes observed by Cluster and their response to changes in plasma parameters, *Journal of Geophysical Research (Space Physics)*, *113*, 4203.

Southwood, D. J., and M. G. Kivelson (1993), Mirror instability. I - Physical mechanism of linear instability, *J. Geophys. Res.*, *98*, 9181–9187.

Tajiri, M. (1967), Propagation of hydromagnetic waves in collisionless plasma. ii. kinetic approach, *Journal of the Physical Society of Japan*, *22*(6), 1482–1494.

Tsurutani, B. T., G. S. Lakhina, O. P. Verkhoglyadova, E. Echer, F. L. Guarnieri, Y. Narita, and D. O. Constantinescu (2011), Magnetosheath and heliosheath mirror mode structures, interplanetary magnetic decreases, and linear magnetic decreases: Differences and distinguishing features, *Journal of Geophysical Research (Space Physics)*, *116*, 2103.

Winterhalter, D., M. Neugebauer, B. Goldstein, E. Smith, B. Tsurutani, S. Bame, and A. Balogh (1995), Magnetic holes in the solar wind and their relation to mirror-mode structures, in *The High Latitude Heliosphere*, pp. 201–204, Springer Netherlands.

The Princeton Plasma Physics Laboratory is operated
by Princeton University under contract
with the U.S. Department of Energy.

Information Services
Princeton Plasma Physics Laboratory
P.O. Box 451
Princeton, NJ 08543

Phone: 609-243-2245
Fax: 609-243-2751
e-mail: pppl_info@pppl.gov
Internet Address: http://www.pppl.gov